Interactive Deformations from Tensor Fields

Ed Boring and Alex Pang
Computer Science Department
University of California, Santa Cruz, CA 95064
edb@cse.ucsc.edu, pang@cse.ucsc.edu

This paper presents techniques for interactively visualizing tensor fields using deformations. The conceptual idea behind this approach is to allow the tensor field to manifest its influence on idealized objects placed within the tensor field. This is similar, though not exactly the same, to surfaces deforming under load in order to relieve built up stress and strain. We illustrate the effectiveness of the Deviator-Isotropic tensor decomposition in deformation visualizations of CFD strain rate. We also investigate how directional flow techniques can be extended to distinguish between regions of tensile versus compressive forces.

Key Words and Phrases: tensor,stress, strain, shear, normal, directional flow, symmetric, antisymmetric, deviator, isotropic.

1 INTRODUCTION

In 1994, Rosenblum [28] hosted a number of papers focusing on "Research issues in scientific visualization". Among the key reports that we found particularly challenging and interesting to our own research and expertise are those by [19] on vector and tensor field visualization. Research on methods for visualizing 2^{nd}-order tensor fields is actively being carried out by a very small group of people: Hesselink [7, 8, 18, 21] in the US, Post [19] and van Wijk [6] in the Netherlands, and Hagen [4, 14] in Germany. Yet scientists and engineers have to deal with these type of data sets almost on a daily basis.

This research presents intuitive, deformation-based tensor field visualization techniques to complement the limited set of current techniques. Deformation is an intuitive and effective method that has been used extensively to illustrate effects of tensile and compressive forces in mechanics textbooks [2]; can be observed directly in nature in the form of geological formations [23]; and alters the molecular alignment of liquid crystals and thus their light scattering capability in order to measure shear stress in compressible flow measurements [27]. Thus, the general idea behind our approach is to embed idealized object(s) (e.g. points, lines, planes, subvolumes) within a tensor field and allow the field to *act upon* the object(s). The result we hope to achieve are deformations (e.g. movements, bending, twisting, compression, elongation, etc.) imposed upon these idealized object(s) by the tensor field. This research investigates visualization methods arising from subjecting idealized objects (surfaces or volumes) to the state information within tensor fields in order to gain an insight into the tensor field. This approach uses fast local computations and yet provides users with a view of the field along extended objects.

We focus on 3-dimensional, 2^{nd}-order tensor fields. This does not unnecessarily limit the applicability of this work since 2^{nd}-order tensor fields (hence referred to as tensor fields) appear in a variety of scientific and engineering applications. Our approach is to develop and evaluate deformation based tensor visualization methods using the Boussinesq problem and other known data sets such as those used in [7, 8]. This is an important and necessary step for validating the correctness of our visualization on a known tensor field, and also useful for comparison with other published tensor visualization methods. We then apply these deformation based techniques to data sets from computational fluid dynamics.

2 PREVIOUS WORK

Tensor fields can be found in numerous physics and engineering applications such as fluid flows [8], mechanics and material science [20], and tectonics [32]. In spite of their prevalence, tools to visualize and understand these data sets are quite limited. In this section, we review the current set of alternatives for visualizing tensor fields.

Pseudo-coloring

This method maps scalar values to color and is used in conjunction with orthogonal planar slices through the volume. Since 3 dimensional 2^{nd}-order tensor fields have 9 scalars at each point, 9 pseudo-colored slices are usually presented in a 3 x 3 panel layout, one for each of the 9 scalar components. The main drawback with this approach is the burden placed on the user to mentally integrate and interpret the 9 separate maps.

Tensor glyphs

This method relies on judicious design and placement of discrete tensor glyphs [12, 6, 26, 24]. Tensor glyphs encode tensor information from discrete locations within the field onto a geometric object. For example, mapping the three eigenvectors as principal axes of an ellipsoid, or including additional derived information such as shear, convergence/divergence, curvature onto a flow probe. Two other techniques that fall under this category are stream polygons [29, 30] and the deformed cube [22]. Both techniques deposit glyphs along a streamline generated from a regular flow field. Stream polygons distorts a polygonal shape according to the local properties derived from a point in a flow field. Similarly, the deformed cube displays a Frenet coordinate frame to show local relative stretch, shear, and rigid body rotation at a point. While glyphs allow the possibility of displaying all the tensor information at a particular point, their principal drawbacks are the loss of continuity from the discrete nature and placement of glyphs, and the potential clutter and overlapping of the glyphs.

Tensor field lines and Hyperstreamlines

Tensor field lines [9] and hyperstreamlines [8] are extensions of vector streamlines into tensor fields. For symmetric tensor fields, the three orthogonal eigenvector components are sorted into largest, median, and smallest eigenvalues. Tensor field lines and hyperstreamlines are then generated by integrating along one of these eigenvector fields. General hyperstreamlines allow the two other eigenvectors and their corresponding eigenvalues to modulate an ellipse along the principal hyperstreamline. For non-symmetric tensor fields, where the three eigenvector components are not necessarily orthogonal to each other, the tensor field is first decomposed into a symmetric tensor field and an accompanying axial vector. Ribbons along the hyperstreamlines are then added to show the rotational effects of the axial vector. Because one of the eigenvector fields is used for integrating the hyperstreamline, there are two other

possible hyperstreamlines that can result from a single seed point. The understanding of the tensor field must therefore be done separately for each eigenvector component, and again the user is left with the burden of integrating and interpreting these three different views.

Topological approach

This approach [18, 21] aims to provide a global structural representation of the tensor field by first identifying degenerate points (trisectors and wedge points) and connecting them with topological skeletons (hyperstreamlines). The result of this approach is a parsimonious display of the important features in the tensor field at the same time showing the continuity (and discontinuities) in the field. Topological tensor field visualization is a direct extension from topological vector field visualization [11, 17, 1]. While this class of methods draws the user's attention to the salient features in the field, the user still has to mentally reconstruct the rest of the field around these degenerate and critical points and skeletons.

Focal surfaces and characteristic curves

Hagen [14] proposes the use of generalized focal surfaces [13] to visualize information derived from real, symmetric deformation tensor fields (e.g. maximum or minimum deformation) on a surface. Directional information is displayed separately by elliptical glyphs placed over characteristic curves. Non-symmetric tensor fields are not supported.

Geodesics

This approach to visualizing symmetric tensor fields is to "construct the geodesics in the Riemannian space determined by the tensor so that the induced curvature can be realized" [10]. Essentially, this method relies on the construction of geodesic surfaces to show the effect of the tensor field as a distortion of flat space. Unfortunately, this method does not easily extend to non-symmetric tensor fields. Furthermore, it is heavily dependent on the efficiency of the numerical methods employed to calculate the geodesics.

3 TENSOR PRIMER

Depending upon the properties being emphasized, a tensor is defined equivalently as an object which obeys a specific transformation rule under a change of coordinate system or as multi-linear map between vector spaces. In our research the second definition is more natural. A 2^{nd}-order tensor quantity is defined to be a bilinear map [5] $\omega \bigotimes \nu$ such that:

$$(\omega \bigotimes \nu) \cdot (\mathbf{a}, \mathbf{b}) = (\omega \cdot \mathbf{a})(\nu \cdot \mathbf{b}) = 1 \tag{1}$$

Here ω and ν are co-vectors, that is, linear maps (dot products) on the vectors $\mathbf{a}$ and $\mathbf{b}$ such that $\omega \cdot \mathbf{a} = 1$ and $\nu \cdot \mathbf{b} = 1$.

In more familiar matrix notation for a 3-dimensional space, Equation 1 allows us to write the expression:

$$\begin{bmatrix} b_1 & b_2 & b_3 \end{bmatrix} \begin{bmatrix} \omega_1\nu_1 & \omega_2\nu_1 & \omega_3\nu_1 \\ \omega_1\nu_2 & \omega_2\nu_2 & \omega_3\nu_2 \\ \omega_1\nu_3 & \omega_2\nu_3 & \omega_3\nu_3 \end{bmatrix} \begin{bmatrix} a_1 \\ a_2 \\ a_3 \end{bmatrix} = 1 \tag{2}$$

Thus, a 2^{nd}-order tensor takes the form of a square matrix and associates state with two directions in space. Provided we have a tensor $\mathbf{T} = \omega \bigotimes \nu$ and the vectors $\mathbf{a}$ and $\mathbf{b}$ we can compute the orginal co-vectors:

$$\begin{bmatrix} \nu_1 \\ \nu_2 \\ \nu_3 \end{bmatrix} = \begin{bmatrix} \omega_1\nu_1 & \omega_2\nu_1 & \omega_3\nu_1 \\ \omega_1\nu_2 & \omega_2\nu_2 & \omega_3\nu_2 \\ \omega_1\nu_3 & \omega_2\nu_3 & \omega_3\nu_3 \end{bmatrix} \begin{bmatrix} a_1 \\ a_2 \\ a_3 \end{bmatrix} \tag{3}$$

and

$$\begin{bmatrix} \omega_1 \\ \omega_2 \\ \omega_3 \end{bmatrix} = \begin{bmatrix} \omega_1\nu_1 & \omega_2\nu_1 & \omega_3\nu_1 \\ \omega_1\nu_2 & \omega_2\nu_2 & \omega_3\nu_2 \\ \omega_1\nu_3 & \omega_2\nu_3 & \omega_3\nu_3 \end{bmatrix} \begin{bmatrix} b_1 \\ b_2 \\ b_3 \end{bmatrix} \tag{4}$$

Indeed, the inner product of $\mathbf{T}$ and any linear combination of $\mathbf{a}$ and $\mathbf{b}$ produces the appropriate linear combination of ω and ν. Thus the tensor is a specific map between the vector space spanned by $\mathbf{a}$ and $\mathbf{b}$ and the vector space spanned by ω and ν.

For example, the stress tensor at a point is a set of components containing stress state information for any arbitrarily oriented plane passing through a point. Multiplication of a unit vector representing a plane normal by the stress tensor gives one of the two *stress vectors* (also known as a *traction vectors*) representing the stress on that plane (Multiplication by the negative normal would yield the second stress vector acting on this plane):

$$\begin{gathered} \mathbf{s} = \boldsymbol{\Sigma} \cdot \hat{\mathbf{n}} \\ s_i = \sigma_{ij}\hat{n}_j \\ \begin{bmatrix} s_1 \\ s_2 \\ s_3 \end{bmatrix} = \begin{bmatrix} \sigma_{11} & \sigma_{12} & \sigma_{13} \\ \sigma_{21} & \sigma_{22} & \sigma_{23} \\ \sigma_{31} & \sigma_{32} & \sigma_{33} \end{bmatrix} \begin{bmatrix} n_1 \\ n_2 \\ n_3 \end{bmatrix} \end{gathered} \tag{5}$$

In this case, we are mapping between the set of 3D plane normals and the set of 3D stress vectors acting on those planes.

Tensors in Fluid Flows

In the study of fluid flows one of the most commonly encountered 2^{nd}-order tensor quantities is the velocity gradient. Indeed, many other useful tensors are derived directly from the velocity gradient, including the rate of strain, viscous stress, stress, reversible momentum flux density, and moment flux density tensor. Hesselink [8] provides a table of these common tensors and their calculation. The velocity gradient is given from the first order Taylor's series expansion of the velocity at a point:

$$\mathbf{V} = \mathbf{V_0} + \frac{\partial \mathbf{V}}{\partial x}\delta x + \frac{\partial \mathbf{V}}{\partial y}\delta y + \frac{\partial \mathbf{V}}{\partial z}\delta z \tag{6}$$

or

$$\mathbf{V} = \mathbf{V_0} + (\nabla \mathbf{V}) \cdot \delta \mathbf{r} \tag{7}$$

where

$$\mathbf{T} = \nabla \mathbf{V} = \begin{bmatrix} \frac{\partial v_x}{\partial x} & \frac{\partial v_x}{\partial y} & \frac{\partial v_x}{\partial z} \\ \frac{\partial v_y}{\partial x} & \frac{\partial v_y}{\partial y} & \frac{\partial v_y}{\partial z} \\ \frac{\partial v_z}{\partial x} & \frac{\partial v_z}{\partial y} & \frac{\partial v_z}{\partial z} \end{bmatrix} \tag{8}$$

Tensor Decomposition

General 2^{nd}-order tensors contain nine independent scalar quantities. It is desirable to reduce this dimensionality in a meaningful way as an aid in understanding the physical state represented by a tensor. Common decompositions include *Symmetric-Antisymmetric* and *Polar Decompositions*. A third decomposition into *Isotropic* and *Deviator* tensors is used to remove a background isotropic contribution which may tend to overwhelm and hide meaningful features found in the Deviator. In our research we have only exploited the Symmetric-Antisymmetric and Deviator-Isotropic Decompositions. They are described in more detail below.

Symmetric-Antisymmetric Decomposition

Any 2^{nd}-order tensor may be decomposed into the sum of a symmetric tensor and an antisymmetric tensor. That is:

$$\mathbf{T} = \mathbf{S} + \mathbf{A} = \frac{1}{2}(\mathbf{T} + \mathbf{T^t}) + \frac{1}{2}(\mathbf{T} - \mathbf{T^t}) \tag{9}$$

Applying this decomposition to the velocity gradient in Equation 8 yields:

$$\mathbf{S} = \begin{bmatrix} \frac{\partial v_x}{\partial x} & \frac{1}{2}(\frac{\partial v_x}{\partial y} + \frac{\partial v_y}{\partial x}) & \frac{1}{2}(\frac{\partial v_x}{\partial z} + \frac{\partial v_z}{\partial x}) \\ \frac{1}{2}(\frac{\partial v_x}{\partial y} + \frac{\partial v_y}{\partial x}) & \frac{\partial v_y}{\partial y} & \frac{1}{2}(\frac{\partial v_y}{\partial z} + \frac{\partial v_z}{\partial y}) \\ \frac{1}{2}(\frac{\partial v_x}{\partial z} + \frac{\partial v_z}{\partial x}) & \frac{1}{2}(\frac{\partial v_y}{\partial z} + \frac{\partial v_z}{\partial y}) & \frac{\partial v_z}{\partial z} \end{bmatrix}$$

$$\mathbf{A} = \begin{bmatrix} 0 & \frac{1}{2}(\frac{\partial v_x}{\partial y} - \frac{\partial v_y}{\partial x}) & \frac{1}{2}(\frac{\partial v_x}{\partial z} - \frac{\partial v_z}{\partial x}) \\ \frac{1}{2}(\frac{\partial v_y}{\partial x} - \frac{\partial v_x}{\partial y}) & 0 & \frac{1}{2}(\frac{\partial v_y}{\partial z} - \frac{\partial v_z}{\partial y}) \\ \frac{1}{2}(\frac{\partial v_z}{\partial x} - \frac{\partial v_x}{\partial z}) & \frac{1}{2}(\frac{\partial v_z}{\partial y} - \frac{\partial v_y}{\partial z}) & 0 \end{bmatrix} \tag{10}$$

The first order Taylor's series expansion of velocity in Equation 6 becomes:

$$\mathbf{V} = \mathbf{V_0} + \mathbf{S} \cdot \delta\mathbf{r} + \mathbf{A} \cdot \delta\mathbf{r} \tag{11}$$

This corresponds to the decomposition of the velocity into local translation $(\mathbf{V_0})$ plus local rate of strain $(\mathbf{S} \cdot \delta\mathbf{r})$ plus local rigid body rotation $(\mathbf{A} \cdot \delta\mathbf{r})$. Since antisymmetric portion $(\mathbf{A})$ is antisymmetric about the diagonal and the diagonal components are 0, it has only 3 independent components, 3 in either the upper triangular matrix or lower triangular matrix. This corresponds to a rotation vector that can be visualized as hedgehogs or ribbons [8] imposed on visualizations of the symmetric tensor. The symmetric part $(\mathbf{S})$ has 6 independent components, 3 in either the upper or lower triangular matrix plus 3 components on the diagonal. This multivariate data is more difficult to visualize.

Isotropic-Deviator Decomposition

A 2^{nd}-order tensor can be decomposed into a Deviator and Isotropic tensor:

$$\mathbf{T} = \mathbf{D} + \mathbf{U}. \tag{12}$$

If $q = \sum_{i=1}^{3} T_{ii}$ (the sum of the diagonal components of $\mathbf{T}$) then:

$$\mathbf{D} = \begin{bmatrix} T_{11} - \frac{1}{3}q & T_{12} & T_{13} \\ T_{21} & T_{22} - \frac{1}{3}q & T_{23} \\ T_{31} & T_{32} & T_{33} - \frac{1}{3}q \end{bmatrix}$$

$$\mathbf{U} = \begin{bmatrix} \frac{1}{3}q & 0 & 0 \\ 0 & \frac{1}{3}q & 0 \\ 0 & 0 & \frac{1}{3}q \end{bmatrix} \tag{13}$$

where $\mathbf{D}$ is the Deviator and $\mathbf{U}$ is the Isotropic tensor.

In the case of the velocity gradient tensor q is equal to $\nabla \cdot \mathbf{V}$, which is the velocity divergence. Thus, for the velocity gradient tensor, the Deviator corresponds to removing $\frac{1}{3}$ of the velocity divergence from each of the diagonal elements. The Isotropic portion can be considered a background that is uniform in every direction, but can dominate over the Deviator [21]. Visualization of the Deviator removes this background and focuses attention on the structure that varies with direction.

Deviator-Isotropic Decomposition can be applied to tensors in general, or to the symmetric part of a Symmetric-Antisymmetric Decomposition. The Deviator has no meaning in the context of the Antisymmetric portion of a tensor since the diagonal elements are null. We utilize the Deviator frequently in our visualizations of the symmetric strain rate tensor.

4 APPROACH

For this research, we focus on symmetric stress tensors from a single point load Boussinesq problem and symmetric strain rate and the Deviator of the symmetric strain rate tensors extracted from CFD data.

Directional Principles

Based on the bilinear mapping of Equation 2, the inner product of a 2^{nd}-order tensor with an arbitrary unit direction vector yields a new *resolute*[1] *vector*:

$$\mathbf{v} = \mathbf{T} \cdot \hat{\mathbf{n}} \tag{14}$$

The form of a 2^{nd}-order tensor is a matrix with order 2 and dimensionality equal to the dimension of our space. For 3 dimensions, our inner product becomes:

$$v_i = \textstyle\sum_j t_{ij} n_j$$

$$\begin{bmatrix} v_1 \\ v_2 \\ v_3 \end{bmatrix} = \begin{bmatrix} t_{11} & t_{12} & t_{13} \\ t_{21} & t_{22} & t_{23} \\ t_{31} & t_{32} & t_{33} \end{bmatrix} \begin{bmatrix} n_1 \\ n_2 \\ n_3 \end{bmatrix} \tag{15}$$

As an example, a stress tensor contains information about the state of stress at a point. The inner product of the stress tensor with a surface normal produces a vector quantity representing the stress on that surface. We can choose any surface normal and thus find the stress on arbitrary surfaces passing through the point. Note that the stress vector for a given surface may have components that are both *shear* and *normal* to the surface. The normal component of stress may be compressive (pushing on to the surface) or tensile (pulling at the surface). In the usual sign convention, if the normal component of stress lies in the half sphere of the surface normal, then it is tensile, otherwise compressive. If the stress vector has no shear component on the surface, then the surface is referred to as *shear free*. If no normal component exists, then the surface is a *plane of maximum shear*.

Other 2^{nd}-order tensor quantities have analogues to the surface normal and the shear/normal components of stress. The vector used in the inner product with a tensor may not represent a surface, but some other directional quantity, such as direction of a magnetic field. Likewise, the analogues to shear and normal stress will vary. For instance plasma flow across magnetic field lines (cross flow) or in the direction of magnetic field lines.

Deviator

We discussed how the Deviator of a tensor removes a sometimes dominant isotropic component from the original tensor. Taking the inner product of the Deviator with a direction vector:

$$\begin{bmatrix} v_1 \\ v_2 \\ v_3 \end{bmatrix} = \begin{bmatrix} t_{11} - \frac{1}{3}q & t_{12} & t_{13} \\ t_{21} & t_{22} - \frac{1}{3}q & t_{23} \\ t_{31} & t_{32} & t_{33} - \frac{1}{3}q \end{bmatrix} \begin{bmatrix} n_1 \\ n_2 \\ n_3 \end{bmatrix}$$

$$= \begin{bmatrix} t_{11} & t_{12} & t_{13} \\ t_{21} & t_{22} & t_{23} \\ t_{31} & t_{32} & t_{33} \end{bmatrix} \begin{bmatrix} n_1 \\ n_2 \\ n_3 \end{bmatrix} - \frac{1}{3}q \begin{bmatrix} n_1 \\ n_2 \\ n_3 \end{bmatrix} \tag{16}$$

shows that the inner product with the Deviator consists of the original tensor inner product minus a constant multiple of the selected direction. The isotropic component present in products with the original tensor is undesirable since it can obscure detail present in

[1] Resolute is borrowed from the vector analysis term representing the scalar product of a vector and a unit normal: $\mathbf{a} \cdot \hat{\mathbf{n}}$

the non-isotropic components. The Deviator is useful in our visualizations since it eliminates this constant multiple of the selected direction and emphasizes the structural detail in the field.

Visualization

To visualize the tensor field we place a geometric object, such as a plane, as an interrogation object [15] in the field. We use trilinear interpolation at discrete points on the surface to obtain tensors at each point. We then form the inner product of the tensors and a user selected vector or vector field (such as the normal to the surface). The derived resolute vector field is then used to visualize the tensor field on the surface.

Our first technique uses the resolute vectors to deform the surface or volume. In this technique, we displace points defining our object by an amount proportional to the resolute vector at that point.

For a point in the original interrogation object $I(\mathbf{x})$ the new point in the deformed object $O(\mathbf{x})$ is given by:

$$O(\mathbf{x}) = I(\mathbf{x}) + s[\mathbf{T}(\mathbf{x}) \cdot \hat{\mathbf{n}}(\mathbf{x})] \tag{17}$$

Position in the field is given by $\mathbf{x}$, s is a scale factor, $\hat{\mathbf{n}}(\mathbf{x})$ is the user selected vector field, and $\mathbf{T}(\mathbf{x})$ are the tensors at each $\mathbf{x}$. The term $\mathbf{T}(\mathbf{x}) \cdot \hat{\mathbf{n}}(\mathbf{x})$ is the resolute vector at $\mathbf{x}$.

The result is an object that is deformed proportional to the resolute vector. For instance, in a stress tensor field, a planar surface with the surface normals chosen for $\hat{\mathbf{n}}(\mathbf{x})$ will force the surface to bulge outward or inward depending upon the magnitude of the normal component of the stress and whether it is compressive or tensile. Note that while such a surface deforms in response to the tensor acting upon it, the resulting deformed surface that we currently obtain in this fashion is not necessarily shear free. Shear stresses will result in expansion or compression of the grid lines forming the surface. If the surface has normal displacement components, this can be seen in the surface image. However, if no normal component exists, viewing a wire-frame of the surface reveals the presence of the shear component (see third image in Figure 1).

In our second technique, we replace the usual surface normals on our surface with the derived resolute vectors. We then visualize the resolute vector field on the surface using directional flow visualization [25, 3] [2]. The resulting visualization highlights areas where the resolute vectors are closely aligned with the visualization light. By changing the direction of the light or surface normal we can quickly identify regions where the resolute vector is shear or normal to the surface (see Color Plate 3). We can also identify compressive versus tensile regions (regions where the derived resolute vector points outward or inward on the surface). One advantage of the directional flow visualization technique is that the lighting model is very sensitive to the direction of the resolute vectors, even if the resolute vectors are of low magnitude.

If we are applying the deformation technique to surfaces, it is useful to select between deformation by (a) the resolute vector (b) or components of the resolute normal, and (c) components of the resolute shear to the interrogation object surface. If we select the entire resolute our deformation is given by Equation 17. If we desire to visualize the normal component of the resolute vector and $\mathbf{r}(\mathbf{x}) = \mathbf{T}(\mathbf{x}) \cdot \hat{\mathbf{n}}(\mathbf{x})$ is the resolute vector, the equation of deformation becomes:

$$O(\mathbf{x}) = I(\mathbf{x}) + s[\mathbf{r}(\mathbf{x}) \cdot \hat{\mathbf{n}}(\mathbf{x})]\hat{\mathbf{n}}(\mathbf{x}) \tag{18}$$

which is deformation by the projection of $\mathbf{r}(\mathbf{x})$ onto $\hat{\mathbf{n}}(\mathbf{x})$ in the direction of $\hat{\mathbf{n}}(\mathbf{x})$. Selecting deformation by the shear component gives:

$$O(\mathbf{x}) = I(\mathbf{x}) + s[\mathbf{r}(\mathbf{x}) - [\mathbf{r}(\mathbf{x}) \cdot \hat{\mathbf{n}}(\mathbf{x})]\hat{\mathbf{n}}(\mathbf{x})] \tag{19}$$

With either the deformation or lighting technique, the surface selection can be translated and rotated within the tensor field. As the surface is moved it will deform or change its shading in response to the tensors present in its new orientation. As with other animation techniques the sense of movement and changing deformation is important in understanding the structure of the tensor field as a whole.

5 IMPLEMENTATION

To investigate a 3D tensor field, the user is provided with a tool to select an arbitrary plane or sub-volume from the 3D tensor volume. The selection tool also allows planes of specified thickness and sub-ranges i.e. sub-volumes of the data set. We then use two different methods to visualize the tensor information from the data subset: surface deformation and extensions to directional flow visualization.

The user may select either (a) the surface normals on the plane or surface of the sub-volume, or (b) a rotatable arrow in space which defines a unidirectional vector field to be used in the inner product with the tensor field. Additional controls are provided to control scaling and clamping of object deformations.

For directional visualization lighting, a second arrow is provided to control lighting direction and a control panel is provided to adjust mapping, focus, and magnitude ranges,

The code implementation is with Java, visualization is done with VTK [30, 31], and tested platforms are on Sun and SGI workstations.

6 RESULTS

Figures 1 to 3 and Color Plates 1 through 5 show visualizations produced with our techniques on a well understood analytical data set and more complicated "real world" data sets generated from CFD simulations.

Validation Tests

Figures 1 to 3 and Color Plate 1 show verification tests performed using a single point load Boussinesq problem data set. This problem is well understood and used by many tensor visualization researchers to illustrate their techniques.

In Figure 1 we show a volumetric data set generated from a single point load Boussinesq problem. The arrow is the direction of applied force. The original geometry is a planar slice perpendicular to the z-axis with positive surface normal in the sense that it is pointing out of the visible face. The surface normal is the selected vector direction whose inner product is taken with the tensors at each point. Resultant stress is used to deform the left image. Middle and right images are deformed by the normal and shear components of the resultant stress respectively. The downward deformation (depressions) seen in images of the resolute and normal component indicate compressive forces (deformation opposite the direction of the normal). Visualization of the shear component in the wireframe image (right most image) shows that shear on this plane is strongest

[2] Directional Flow Visualization maps the angular deviation of a vector field from a selected light vector to hue or value in an HSV pseudo-color map. Typically, a direction-to-hue map is utilized with red hues indicating that the vector field in a region is aligned with the light direction, and blue-magenta hues indicate a vector field perpendicular to the light direction. The mapping and illumination controls allow the user to select a direction or range of directions of interest. For instance, it is possible to illuminate all vectors perpendicular to the light, or all vectors aligned within a small angular cone of the light direction. The technique is highly sensitive to directional variation in a field and can be used to distinguish shear, normal, anti-normal, and in between states of the vector field directions relative to the light.

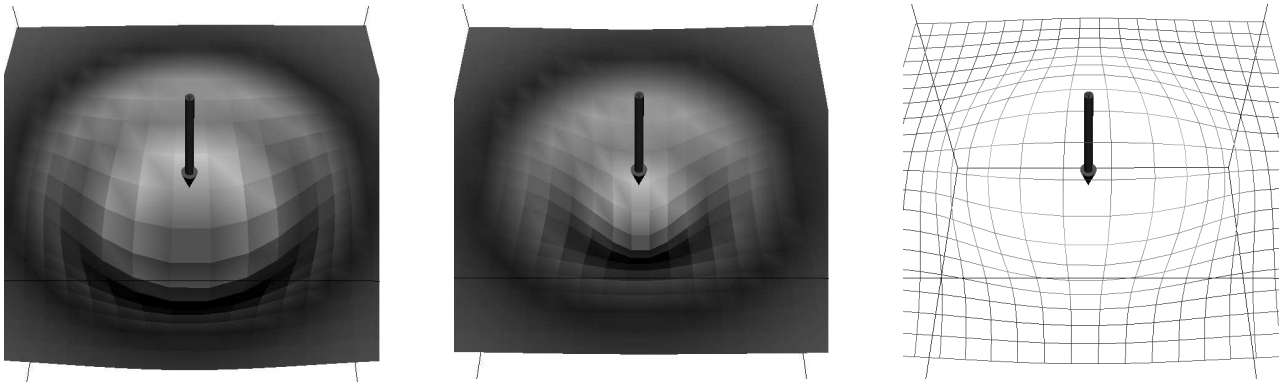

Resultant stress. Normal stress component. Shear stress component.

Figure 1: Single point load Boussinesq problem - surface deformation of a z-axis slice

toward the center of the plane and decreases as we move to the outer edges of the plane.

Figure 2 illustrates the improvement in resolving the non-isotropic details by using the Deviator tensor. Figure 2 shows the same tensor field as in Figure 1, but now resolved on a plane perpendicular to the x-axis. The plane normal is along the positive x-axis pointing to the right in the images. The view is from the top looking down along the z-axis. At the top of the plane, we have two "fans" of displacement. The one to the right is at the very top and represents a tensile stress in the direction of the surface normal. The "fan" on the left is just below the first and represents a compressive stress. In the left image we show the stress with both isotropic and deviator components present. The right image is produced after removal of the isotropic tensor leaving only the deviator of the stress tensor. The compressive fan (pointing to the left) is clearly smaller in the right image with the isotropic component removed. This indicates an isotropic component that is negative. Close observation of the right image reveals a slight curvature of the planar slice above and below the "fans" in the direction of the surface normal representing tensile stress. In the left image where a negative isotropic component exists in this region, the curvature is reduced.

In Figure 3 and Color Plate 1 we compare our deformation technique with hyperstreamlines. The hyperstreamlines are integrated through the minor eigenvector field and show the propagation of the most compressive forces. Two planar z-axis slices at different positions are deformed in the field using the positive surface normal as the direction vector field. Hyperstreamlines clearly show the direction of greatest compression and, through pseudo-coloring by the eigenvalue, the magnitude of the compressive forces. Deformed planes give a stronger visual clue about the relative magnitude of forces. Additionally, they cover a large region of the field and hence provide more direct information over a greater portion of the field.

Delta Wing

Color Plates 2 and 3 visualize the strain rate deviator tensor field on a grid slice extracted from the computational grid perpendicular to and just behind a delta wing at a 40 degree angle of attack (http://science.nas.nasa.gov/Software/DataSets). Since the delta wing is symmetric about its central axis, the computational data sets (and consequently visualizations from the data set) contain only the left half of the wing geometry shown by portions of the magenta triangle in each of the images. Our images show a portion of the computation grid (greenish rectangular shape abutting the magenta wing) behind the actual delta wing. This portion of the grid is in the same plane as the delta wing surface and is an artifact generated from the extraction of delta wing geometry from the computational grid.

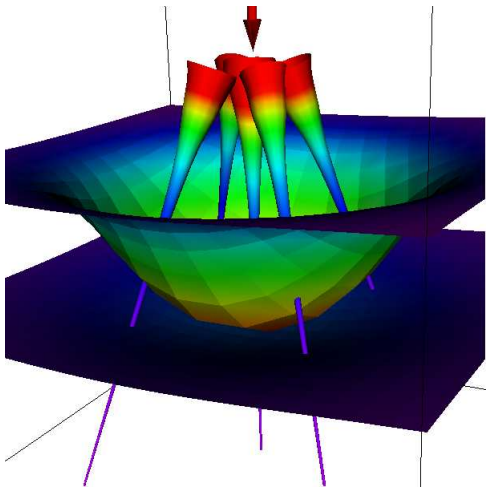

Figure 3: Single point load Boussinesq problem - Two z-axis slices and minor hyperstreamlines

Color Plate 2 provides various viewing angles of the normal component of the strain rate Deviator on the flow field slice behind the delta wing. The slice is pseudo-colored by velocity magnitude. A vortex that forms above and extends behind the wing surface is indicated by the magenta pseudo-colored region on the deformed grid slice in the images. To produce the deformation, a negative surface normal pointing opposite the visible face in the left most image is used as the direction vector field. As such, depressions in the left most image represent tensile strain and extrusions toward the viewer represent compressive strain.

A frontal view is presented in the left image with the tip of the delta wing (partial magenta triangle) off the lower right corner of the frame. The middle image is viewed from above looking down onto the plane of the delta wing with the tip of the delta wing off the bottom of the frame. Finally, the right image is posterior with the tip of the delta wing off the upper right hand corner of the image. At the base of the slice near the delta wing surface we observe region of tensile strain whose extent can be seen in the posterior view and the top view. A compressive region is indicated by the extrusion seen on the right hand side of the slice in the left and middle images. A tensile strain region is seen near the left side and base of the wing where there is separation of the flow from the wing as it begins to form a vortex. In the vortex core (blue region with magenta center) we note a tensile strain. To the right and below the vortex core is a

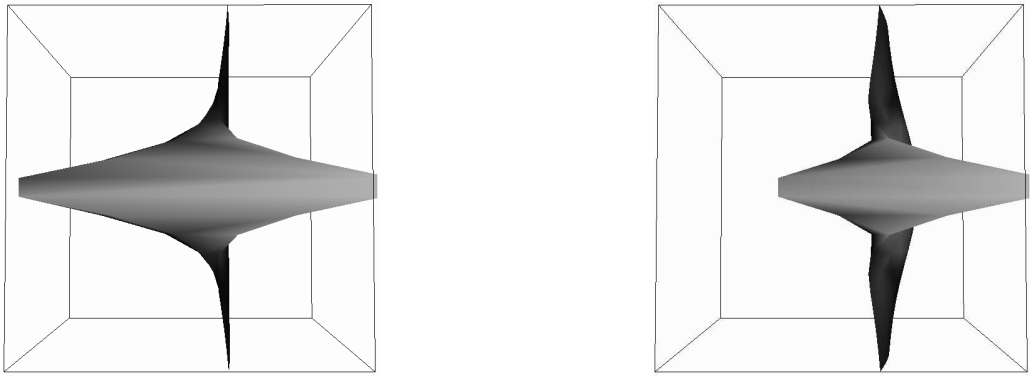

Stress tensor. Deviator of stress tensor.

Figure 2: Single point load Boussinesq problem - Deviator/Isotropic comparison on x-axis slice

compressive region.

Color Plate 3 illustrates directional visualization of the strain rate Deviator. The yellow arrow indicates the light vector and is normal to the grid slice surface. The vector field being illuminated is computed from the inner product of the strain rate Deviator and the surface normal. A direction-to-hue color map is employed with red hues indicating resolute vectors closely aligned with the light direction and blue-magenta hues indicating directions with a large angular separation from the light. The left and middle images use a focus of 0-90 degrees so magenta hues indicate a resolute vectors perpendicular to the light and thus primarily shear strain. Dark regions indicate resolute vectors with an angular separation greater than 90 degrees from the light.

Negative surface normals pointing opposite the visible face are selected for the direction field in the middle and right images. Thus, lit regions possess a compression component with red indicating most compressive and least shear, while magenta regions exhibit mainly shear. Note that no hint of the relative magnitude of the resolute vectors is given, only the directional quality.

The left image uses a positive surface normal (toward the viewer from the visible face) as the direction field. In this case tensile, rather than compressive, strain is visible as orange and red hues, while shear strain appears in blue-magenta hues. Again, as in the middle image, dark areas indicate resultant strain that at greater than 90 degrees from the light, in this case indicating at least some compressive component.

Finally, the right image attempts to combine visualization of both compressive, tensile, and shear components in the same directional visualization image. Here, a negative surface normal (pointing opposite the visible face) is selected as a direction vector field. A focus of 0-180 degrees in chosen so that resolute vectors in the direction of the light, and hence compressive, are pseudo-colored red, while resolute vectors opposite the light, and hence tensile, are pseudo-colored magenta. Green and cyan hues represent vectors perpendicular to the light and are visible in regions that posses primarily shear strain.

Features visible in these images include a tensile strain region near center of the slice associated with eye of a vortex. Shear strain is visible surrounding the vortex eye, at the base of the slice where it touches the same plane as the wing, and along a band on the left of the slice where the flow is lifting and beginning to spiral toward the vortex. Large tensile and compressive regions are also clearly visible.

Hemispherical Cylinder

Color Plates 4 and 5 illustrate our deformation technique applied to a hemispherical cylinder at 40 degree angle of attack CFD data set. The surfaces are HSV pseudo-colored by velocity magnitude.

Color Plate 4 illustrates deformation by the resolute of the strain rate deviator on the hemispherical cap at the top of the cylinder. The free stream flow is striking the cylinder from the top in these images. Undeformed geometry is shown in the left image while the right image is deformed using outward pointing surface normals as the direction vector field. Though it may appear that the majority of the deformation is normal to the original surface, it is in fact almost entirely shear. The "expanded" appearance of the cap is due to a steadily increasing shear component from the head of cap to the cylinder body. The ability to rapidly select between shear, normal, and resolute strain in the visualizations tools reveal this detail. The hole at the tip of the of the cap is excluded geometry due to difficulties in calculating the tensor gradient in this region, but it provides a reference point to compare between the two images. Notice that the shape of the excluded geometry deforms from circular to oval indicating a shear in this region. An interesting feature originates from the small magenta colored region (with the shape of a tiny downward pointing spike) just below the circular area of excluded geometry. Carefully comparing the two images reveals that this region has been strongly deformed left, right and downward giving the appearance of the "lip".

Color Plate 5 illustrates visualization of a grid slice perpendicular to the body of the hemispherical cylinder. Here the cylinder has been rolled around its axis by 180 degrees from the images in Color Plate 4, in this case the free stream flow strikes the bottom of the cylinder. The surface normals point to the right in each image and are used as the direction vector field for the deformations The left image is deformed by the normal component of the strain rate tensor, while the middle image shows deformation by the normal component of the strain rate deviator. The right most image shows directional visualization of the resolute on the undeformed slice with a focus of 0-180 degrees. Several compressive (to the left) and tensile (to the right) spikes can be seen below the cylinder. Careful comparison of the deformation images show a number of subtle differences. Below the cylinder there is a strong negative isotropic component which depresses the geometry to the left giving a smoother appearance than the deviator alone. This is an example where the isotropic component overwhelms details present in the deviator. On the side of the cylinder body tensile compression results in a cuff that reaches its maximal extent at the cylinder midpoint. The extents and shapes of these cuffs are dominated by isotropic elements in the the left image but not in the middle image.

Directional visualization in the right image reveals concentric rings of alternating shear, compressive, and and tensile regions. Because the light and normal point to the right of the image, red hues match regions of tensile strain, magenta indicates compres-

sive strain, and green/cyan indicate largely shear strain. Near the cylinder body we observe mostly shear strain indicated by the cyan pseudo-color. Moving outward from the cylinder body we observe a ring of shear strain, followed by a compressive ring, followed by a tensile ring and finally a transition back to compressive strain.

Issues

By themselves, 2D still images produced by this technique are not as useful as visualizations produced in the interactive environment. Deformed surface structures are most often complex for real world data and it is necessary to rely upon animation and rotation to form a mental picture of the structure. It is useful to interactively change the scale of deformation and displace the initial geometry to observe tensor field changes through the field. The use of interactive directional lighting helps identify small changes in the direction of the resolute field. Additionally, care must be taken when the initial geometry is non-planar. It is often necessary to select between shear and normal deformation since a deformation may at first appear to be normal to a surface when in reality it may be almost entirely shear as discussed in reference to Color Plate 4.

Another problem is the frequent generation of non-manifold (self-intersecting) geometry from deformations. This is particularly true in the presence of strong shear components. Methods we have used for dealing with this problem include interactively adjusting the deformation scale, logarithmic scaling or clamping of the deformation, and adjusting the geometry to separate visualization of regions with strong self-intersecting deformation from regions of smaller deformation. We also rely upon directional lighting rather than deformation in some cases. Other possible techniques would include limiting the deformation to some fraction of the actual grid size of the initial geometry or attempt some form of non-manifold geometry detection. The drawbacks are that the deformations would become small for finely structured geometry and non-manifold geometry detection would degrade interactivity.

7 FUTURE WORK

In our current implementation we have focused on deforming planar surfaces, either cutting planes or planar extractions of the data grid. These test geometries are limited but the techniques could easily be extended to operate on isosurfaces of scalar values (such as the locus of eigenvalues which meet various conditions), spherical or cylindrical shapes, or complex geometries modeled with implicit functions. Any surface or volumetric geometry that is suitable for a particular problem could be utilized.

Both the deformation and directional visualization technique have the advantage of not being limited to symmetric tensors as many tensor visualization techniques are. By re-orienting the surface selection in the field, or changing the order of the inner product, antisymmetric tensors of the field can be observed. For instance, by rapidly flipping a planar surface so that the surface normal is negated, it should be possible to observe antisymmetry in the tensors, particularly if there is a pattern of antisymmetry (rotation) in the whole field. More work needs to be done in this area to determine if antisymmetry is clearly visible using this technique, as well as investigating other techniques, such as 4D lights [16], for this purpose.

We have not investigated visualization using the Polar Decomposition. We believe that in the physical situations where the Polar Decomposition is permitted (the determinate of the original tensor must be 0), the Polar Decomposition will provide further clues about the behavior of the field. In the Polar Decomposition, the stretch component maintains more amplitude information than in the Symmetric-Antisymmetric decomposition. Thus, tensor inner product of the stretch component and the direction field should carry more of this information and be visible in the resulting deformations.

The electronic version of this paper and additional images are available at www.cse.ucsc.edu/research/avis/tensor.html.

8 CONCLUSIONS

This research has focused on visualizing the symmetric portion and the Deviator portion of real 2^{nd}-order tensor fields using deformation of idealized objects placed in the field. By providing the user with a controllable geometry and direction vector field, the tensor field can be explored interactively in many directions and over large extended regions of the field. This provides direct visual clues and an overall sense of the tensor field behavior. Compressive and tensile regions of symmetric tensors are resolved as extrusions and depressions in the deformation of surfaces. Shear components can be seen in wire-frame images or as expansions and compressions of the geometry tangent to object surfaces placed in the field.

Visualization of complex tensor fields is enhanced by using the Deviator-Isotropic decomposition. The decomposition allows removal of isotropic (unidirectional) components in the field and reveal more of the structure that is directionally dependent.

Directional flow visualization is highly sensitive to the directional information in a resolute vector field produced from the inner product of the the tensor field and a direction vector field. It is effective in revealing regions of tensile, compressive, and shear effects, as well as states in between pure normal and pure shear.

ACKNOWLEDGEMENTS

We would like to thank Steve Ward of the UCSC Earth Science Board for his input concerning tensors and tensor visualization in the Geophysical sciences, and David Kenwright of NASA/Ames for his input and discussion on tensors and tensor visualization in Aerodynamics. We would like to thank the Santa Cruz Laboratory for Visualization and Graphics (SLVG) for the wonderful research environment. This project is supported by NSF grant IRI-9423881, NASA Cooperative Agreement NCC2-5207, ONR grant N00014-92-J-1807, and DARPA grant N66001-97-8900.

References

[1] Daniel Asimov. Notes on the topology of vector fields and flows. Technical Report NASA-RNR-93-003, NASA Ames Research Center, 1993.

[2] Maurice Biot. *Mechanics of Incremental Deformations*. Wiley, 1965.

[3] Ed Boring and Alex Pang. Directional flow visualization of vector fields. In *Proceedings of Visualization 96*, pages 389–392, October 1996.

[4] Manfred Brill, Hans Hagen, Hans-Christian Rodrian, Wladimir Djatschin, and Stanislav V. Klimenko. Streamball techniques for flow visualization. In *Proceedings of Visualization 94*, pages 225–231. IEEE Computer Society, 1994.

[5] William L. Burke. *Applied Differential Geometry*. Cambridge University Press, 1985.

[6] Willem C. de Leeuw and Jarke J. van Wijk. A probe for local flow field visualization. In *Proceedings of Visualization 93*, pages 39–45. IEEE Computer Society Press, October 1993.

[7] T. Delmarcelle and L. Hesselink. Visualization of second order tensor fields and matrix data. In *Proceedings of Visualization 92*, pages 316–323, CP–34, 1992.

[8] T. Delmarcelle and L. Hesselink. Visualizing second-order tensor fields with hyperstreamlines. *IEEE Computer Graphics and Applications*, 13(4):25–33, July 1993.

[9] R. R. Dickinson. A unified approach to the design of visualization software for the analysis of field problems. In *SPIE: Three-Dimensional Visualization and Display Technologies*, volume 1083, pages 173 – 180, 1989.

[10] R. K. Dodd. A new approach to the visualization of tensor fields. *Draft copy*, February 1996.

[11] Al Globus, Creon Levit, and Tom Lasinski. A tool for visualizing the topology of three-dimensional vector fields. In *Proceedings: Visualization '91*, pages 33 – 40. IEEE Computer Society, 1991.

[12] R.B. Haber and D.A. McNabb. Visualization idioms: a conceptual model for scientific visualization systems. In *Proceedings of IEEE '90 Visualization*, pages 74–93. IEEE, 1990.

[13] H. Hagen and S. Hahmann. Generalized focal surfaces: A new method for surface interrogation. *Proceedings of IEEE Visualization '92*, pages 70–76, 1992.

[14] H. Hagen, S. Hahmann, and H. Weimer. Visualization of deformation tensor fields. In G. Nielson, H. Hagen, and H. Muller, editors, *Scientific Visualization: Overviews, Methodologies, Techniques*, pages 357–371. IEEE Computer Society, 1997.

[15] Hans Hagen, Stefanie Hahmann, Thomas Schreiber, Yasuo Nakajima, Burkard Wordenweber, and Petra Hollemann-Grundstedt. Surface interrogation algorithms. *IEEE Computer Graphics and Applications*, 12(5):53–60, September 1992.

[16] A. Hanson and H. Ma. Visualizing flow with quaternion frames. In *Proceedings of Visualization 94*, pages 108–115. IEEE Computer Society, 1994.

[17] J. L. Helman and Lambertus Hesselink. Visualization of vector field topology in fluid flows. *IEEE Computer Graphics and Applications*, 11(3):36–46, 1991.

[18] L. Hesselink, Y. Levy, and Y. Lavin. The topology of symmetric, second-order 3d tensor fields. *IEEE Transactions on Visualization and Computer Graphics*, 3(1):1–11, Jan-Mar 1997.

[19] L. Hesselink, F. Post, and J.J. van Wijk. Research issues in vector and tensor field visualization. *IEEE Computer Graphics and Applications*, 14(2):76–79, March 1994.

[20] R.D. Kriz, E.H. Glaessgen, and J.D. MacRae. Visualizing gradients in composite design and fabrication. *IEEE Computer Graphics and Applications*, 15(6):10–13, November 1995.

[21] Y. Lavin, Y. Levy, and L. Hesselink. Singularities in nonuniform tensor fields. In *Proceedings of Visualization 97*, pages 59–66, 1997.

[22] Xundong Liang, Bin Li, and Shenquan Liu. The deformed cube: a visualization technique for 3d velocity vector field. In *Image Analysis Applications and Computer Graphics. Third International Computer Science Conference. ICSC'95*, pages 51–58. Springer, 1995.

[23] Richard Lisle. *Geological Structures and Maps, A Practical Guide, 2nd Edition*. Butterworth-Heinemann, 1995.

[24] M. Livingston. Visualization of rotation fields. In *Proceedings of Visualization 97*, pages 491–494, 584, 1997.

[25] Alex Pang and Naim Alper. Bump mapped vector fields. In *SPIE & IS&T Conference Proceedings on Electronic Imaging, Vol. 2410: Visual Data Exploration and Analysis II*, pages 78–86, color plate page 205. SPIE, February 1995.

[26] F. J. Post, T. van Walsum, F. H. Post, and D. Silver. Iconic techniques for feature visualization. In *Proceedings Visualization '95*, pages 288–295, Atlanta, GA, November 1995. IEEE.

[27] D. Reda, J. Muratore Jr., and J. Heineck. Time and flow-direction responses of shear-stress-sensitive liquid crystal coatings. *AIAA Journal*, 32(4):693–700, April 1994.

[28] L. J. Rosenblum. Research issues in scientific visualization. *IEEE Computer Graphics and Applications*, 14(2):61–63, March 1994.

[29] W. J. Schroeder, C. R. Volpe, and W. E. Lorensen. The Stream Polygon: A technique for 3D vector field visualization. In *Proceedings: Visualization '91*, pages 126 – 131. IEEE Computer Society, 1991.

[30] Will Schroeder, Ken Martin, and Bill Lorensen. *The Visualization Toolkit: An Object-Oriented Approach to 3D Graphics*. Prentice Hall, New Jersey, 1996.

[31] W.J. Schroeder, K.M. Martin, and W.E. Lorensen. The design and implementation of an object-oriented toolkit for 3d graphics and visualization. In *Proceedings of Visualization 96*, pages 93–100, 472. ACM, 1996.

[32] Seth Stein. *Introduction to seismology, earthquakes, and earth structure*. Draft copy, 1991.